The Planetary Science Journal, 2:169 (9pp), 2021 October https://doi.org/10.3847/PSJ/ac13a3

Siderite Dissolution in Mars-analog Brines: Kinetics and Reaction Products

M. D. Cullen[1], C. M. Phillips-Lander[2], A. S. Elwood Madden[3], and M. E. Elwood Madden[3]
[1] Oklahoma Geological Survey, Norman, OK, USA
[2] Southwest Research Institute, San Antonio, TX, USA
[3] School of Geosciences, University of Oklahoma, Norman, OK, USA
Received 2021 March 22; revised 2021 June 21; accepted 2021 June 22; published 2021 August 24

Abstract

This study examines siderite ($FeCO_3$) reactivity in $MgCl_2$ and $MgSO_4$ brines with varying salt concentrations (0.01M, 1M, and 3M) at both acidic (pH $\sim$ 2 and pH $\leqslant$ 2) and near-neutral (pH $\sim$ 7) conditions. We measured aqueous Fe concentrations through time to determine dissolution rates and characterized the solid reaction products with scanning electron microscopy, electron dispersive X-ray spectroscopy, and Raman spectroscopy. Iron-based siderite dissolution rates at pH 2 were equivalent in the 0.01M and 1M $MgSO_4$ brines and slower in 3M $MgSO_4$; rates in the $MgCl_2$ brines slow systematically with increasing brine concentration for equivalent initial pH values. Fe-based dissolution rates could not be determined in the neutral pH experiments due to precipitation of iron (hydr) oxide phases. After 1 day in acidic brines, abundant etch pits were observed; however, in the neutral experiments, siderite was identified with Raman spectroscopy even after 1 yr of dissolution along with a range of iron (hydr) oxide phases. Scanning electron microscopy imaging of the neutral experiment products found Mg-sulfate brines produced a chaotic surface texture. Therefore, micron-scale textural observations could be used to discriminate between alteration in chloride and sulfate brines. Initial iron release rates were similar in dilute brines, but decreased by less than an order of magnitude in the two highest-concentration pH 2 brine experiments; therefore, siderite-bearing assemblages exposed to acidic fluids, regardless of salinity, would likely dissolve completely over geologically short periods of time, thus erasing siderite and likely other carbonate minerals from the geologic record.

Unified Astronomy Thesaurus concepts: Mars (1007)

Supporting material: data behind figure

1. Introduction

Widespread salt deposits observed on the surface and mixed with near-surface regolith provide evidence that salty liquid water has been active on Mars. These brines likely formed by evaporation or freezing (Osterloo et al. 2010; Ojha et al. 2015). Additionally, atmospheric and climate data suggest that modern aqueous liquids may be present on a diurnal or a seasonal basis (Martín-Torres et al. 2015; Rivera-Valentín et al. 2020). This implies that geochemical processes such as mineral alteration and dissolution in brines have likely occurred at or near the surface throughout Mars history and may still be occurring today.

Data obtained by CRISM indicate, among other phases, the presence of magnesium chlorate/perchlorate salts in modern recurring slope linea (Ojha et al. 2015), as well as widespread sulfate and chloride assemblages in older rocks (Clark et al. 2005; Ehlmann et al. 2008). Rocks, sediments, and soils observed on the surface include various phosphate, sulfate, chloride, and carbonate minerals (Squyres et al. 2004; Morris et al. 2010; Osterloo et al. 2010; Adcock et al. 2013; Hausrath & Olsen 2013). Chloride salts likely formed as a result of precipitation, volcanism, or impact processes during the Noachian and Hesperian (Osterloo et al. 2010). Among the observed sulfate phases are jarosite and alunite, which both indicate acidic aqueous conditions (Elwood Madden et al. 2004; Ehlmann et al. 2016; Miller et al. 2016). Polyhydrated sulfate phases are also observed and can be indicators of atmospheric water vapor pressure, as well past aqueous activity (Cloutis et al. 2007; Wang et al. 2016). The presence of acidic pH environmental indicators such as jarosite also imply that many rocks at the surface of Mars were likely in contact with acidic aqueous fluids at some point in Mars history, and may continue to be in intermittent contact with such fluids even today (Yen et al. 2005; Martín-Torres et al. 2015).

Siderite ($FeCO_3$) has been observed both on the surface of Mars in outcrops (Ehlmann et al. 2008; Sutter et al. 2012; Hausrath & Olsen 2013) and in SNC meteorites (Bridges et al. 2001); however, carbonates are less abundant than would be expected given the high CO_2 concentration of the Martian atmosphere (Ehlmann & Edwards 2014). Previous studies have suggested that acidic fluids, believed to have been dominant during the late Noachian, may have dissolved much of the original carbonates at the surface leading to the sparsity observed today (Ehlmann et al. 2008; Sutter et al. 2012). However, the detection of carbonates, including siderite, in the Phoenix lander sediments indicates the presence of circumneutral pH conditions (Sutter et al. 2012). Therefore, carbonate preservation across Mars's surface may reflect heterogeneous geochemical and/or climate conditions (Sutter et al. 2012).

Bibring et al. (2006) posit that early Martian history was dominated by neutral alteration producing phyllosilicates, which was then followed by volcanism and acidic sulfate alteration. It has also been proposed that interactions between a CO_2-rich atmosphere and large bodies of sulfate- and iron-dominated aqueous solutions would lead to mildly acidic pH (5.3–6.2) conditions as early as the Noachian (Fairén et al. 2004). Due to photolytic oxidation of aqueous Fe^{2+} to the 3+

state, the equilibrium pH could fall as low as 2, preventing carbonate formation and resulting in carbon primarily existing as atmospheric CO_2 (Fairén et al. 2004). Given that Mars likely experienced both acidic and circumneutral (pH 5–8) aqueous conditions at different times in its history, and there is abundant evidence of salts on the surface of Mars, this study aims to examine the kinetics and reaction products of siderite in magnesium-bearing brines with varying anion chemistry at different pH conditions to determine how these factors affect siderite dissolution and preservation.

2. Methods

We prepared anaerobic $MgCl_2$ and $MgSO_4$ brine solutions from pH 2 stock solutions of HCl (for the pH 2 $MgCl_2$ brines) and H_2SO_4 (for the pH 2 $MgSO_4$ brines) and ultrapure water (UPW) for the neutral solutions. We chose Mg-based brines because magnesium sulfate minerals appear to be abundant on Mars (Gendrin et al. 2005) and magnesium chloride brines have very low melting temperatures (Toner et al. 2014) and evaporation rates (Altheide et al. 2009) allowing them to remain liquid over a wide range of temperature and pressure conditions. We also chose these two brine compositions in order to directly compare the effects of anion composition on dissolution rates.

We removed dissolved O_2 by boiling the stock solutions and then exposing them to flowing N_2 while cooling to prevent diffusion of O_2 back into solution. Then we transferred the neutral and acidic solutions into an anaerobic chamber. For each pH condition, we prepared 250 ml of solution, then added the requisite mass of salt to make 0.1 M, 1 M, and 3 M salt solutions. This yielded 12 unique solutions, with differing pH ($\leqslant 2$ or near-neutral), salt composition ($MgCl_2$ or $MgSO_4$), and salt concentration (0.1 M, 1 M, or 3 M). The initial pH of the $MgCl_2$ experiment solutions decreased after adding the $MgCl_2$ salts; therefore, experiments were duplicated using the same methods but then we readjusted the pH to 2 after adding the salt. Therefore, the $MgCl_2$ experiments resulted in two data sets: one at pH 2 and one where the initial pH of the brines decreased with increasing salinity.

We micronized a natural sample of siderite obtained from a mineral dealer (composition confirmed with powder X-ray difraction (XRD)) using a McCrone mill, rinsed the material with ultrapure water, and then measured the surface area of the starting material (0.6 $m^2\,g^{-1}$) with a Quantachrome Nova 2000e nitrogen-adsorption surface area analyzer, using the Brunauer–Emmett–Teller (BET) method. We added 0.075 ± 0.005 g siderite and 75 ml of brine to brown serum vials (to minimize photolytic reactions) before capping and sealing them within the anaerobic chamber. The serum bottles were then removed from the anaerobic chamber and placed on an orbital shaker for seven weeks.

Experiments were conducted in duplicate, resulting in 36 reactors, 12 reactors for each pH condition. Sampling (5 ml each) took place weekly using needled syringes to collect the solid–liquid slurry, while maintaining anaerobic conditions within the reactor. The samples were filtered using 0.2 μm acetate syringe filters. We measured pH of the acidic brines using a 2 ml subsample, then saved the remainder for later analyses. Samples from the neutral pH experiments were acidified after sampling with either HCl or H_2SO_4, matching the brine anion, to prevent precipitation of aqueous Fe after sampling. At the end of the experiment, we analyzed dissolved total Fe concentrations in each sample using matrix-matched flame atomic absorption spectroscopy calibrated with known standards, yielding a detection limit of $\sim 10^{-5}$ mol kg^{-1} Fe. We measured the Fe concentrations in the experimental blanks (unreacted brine) and subtracted these concentrations from the Fe measured in the dissolution samples to account for trace iron concentrations in the salts. The resulting Fe concentrations were normalized to the BET surface area to determine the concentration of Fe released from a known surface area of siderite and plotted as a function of time. We fit the first four sample points with a second-order polynomial, then differentiated the polynomial to determine the initial dissolution rate in the acidic experiments (Figure 1) following the method described in Rimstidt (2014). However, the neutral experiments produced Fe concentrations that were similar or less than the experimental blanks, thus initial rates could not be determined in the neutral experiments (neutral pH data available in the data behind Figure 2).

We analyzed both the unreacted micronized siderite and the solid reaction products using Raman spectroscopy and scanning electron microscopy (SEM). Samples were rinsed through a vacuum filter and analyzed using a Renishaw InVia high-resolution Raman microscope with a 500 mW 785 nm red laser at 0.0001% power to minimize the effect of laser heating on iron oxide mineralogy. We collected spectra for 180–300 s using a 50× objective and a 1200 l mm^{-1} grating centered at 700 cm^{-1} to yield spectra from 100 to 1300 wavenumbers. We subtracted the baseline and normalized the intensity using the WiRe 4.1 software and then compared the spectra to known minerals using the RRUFF database (Lafuente et al. 2015) and the existing literature. Samples that had been stored in the brine for a year or more (364 days for the neutral experiments and 552 days for the pH $\leqslant 2$ acidic experiments) were also analyzed to further study the reaction products after longer-term exposure to brines.

We used a Zeiss Neon EsB Field-Emission SEM at an accelerating voltage of 15 kV to capture images at consistent magnifications. We used these images to compare dissolution textures in the samples reacted for $\sim$15 weeks in the neutral brines and 1 day in the acidic brines. We prepared the 1 day acidic chloride reactors using the unadjusted pH solutions. We used energy dispersive X-ray spectroscopy (EDX) to obtain chemical analyses of various sites on the surface of grains in each sample.

3. Results

3.1. Aqueous Dissolution Rates

Aqueous Fe concentrations increase steadily over the first 2–5 samples in the acidic dissolution experiments in both the $MgCl_2$ and $MgSO_4$ brines. Fe concentrations plateau after these first few samples, suggesting that the siderite dissolves readily in the acidic brines over the first 1–25 days of reaction, then the siderite either is consumed, reaches equilibrium with the aqueous solution in the batch reactors, or reaches a steady state as iron (hydr)oxides precipitate; pH in the acidic experiments was observed to increase with time from initial pH = 2 or less to pH = 3–4.5. Therefore, we used only the first few data points to calculate Fe-based dissolution rates in the acidic experiments (Figure 1).

We repeated the chloride brine experiments with slightly different brine conditions, once at an initial pH of 2 in all of the

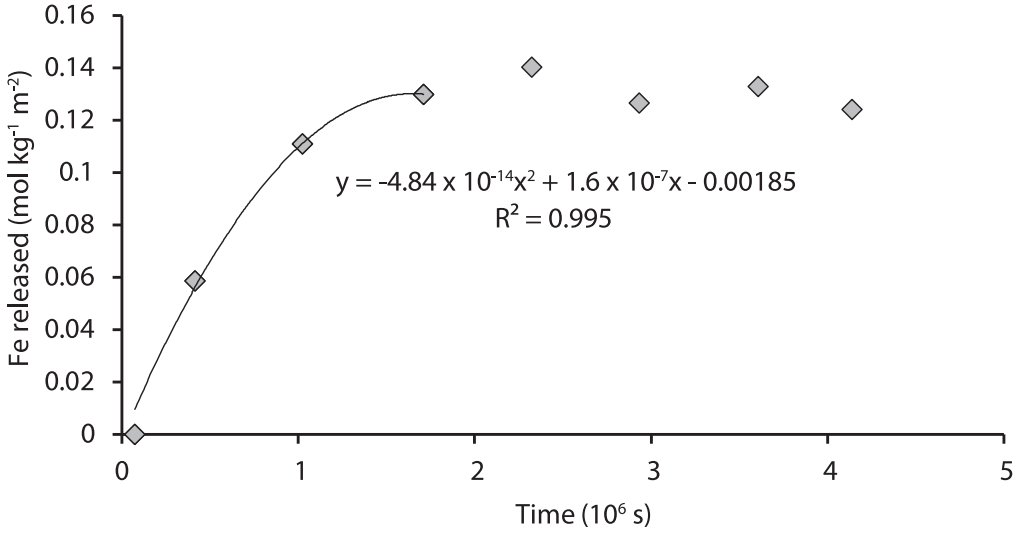

Figure 1. Aqueous Fe concentration vs. time example from an acidic experiment. Concentration has been normalized to the BET surface area of the original sample and the first four data points fit with a second-order polynomial in order to determine the initial rate. Concentrations plateau after the fourth sampling point as the experiment reaches steady state.

reactors and once at lower pH values, depending on brine strength (Table 1; Figure 2). In our initial experiments, the pH dropped as we added chloride salts to the pH 2 HCl, reaching as low as 0.29. We ran a second set of experiments where we readjusted the pH of the brine to 2 after adding the salts. Thus, there are a set of $MgCl_2$ experiments all at a pH of 2 and a set with an initial pH < 2. Overall, siderite dissolution rates generally decreased with increasing $MgCl_2$ concentration when pH was constant (Figure 2(D)). However, when both acidity and salt concentration increased dissolution rates increased slightly, likely as a result of decreasing pH (Figure 2(B)). In the sulfate experiments, siderite dissolution rates were similar in the 0.01 M and 1.0 M brines and slowest in the 3.0 M brine (by less than an order of magnitude; Figure 2(A)). Dissolution rates could not be determined using the aqueous Fe concentrations observed in the neutral experiments since Fe concentrations did not vary systematically.

3.2. Reaction Products and Textures

In addition to the aqueous Fe data, we also collected SEM images and EDX spectra from surfaces of the grains after dissolution. We initially analyzed the siderite after 15 weeks of dissolution in the near-neutral pH brine experiments, since we could not determine dissolution rates with the aqueous iron data.

SEM images of the 15 week neutral experiments show that dissolution texture varies significantly between the two brine compositions (Figure 3). In the chloride experiments, the siderite surface becomes increasingly worn and jagged as $MgCl_2$ concentration increases. Higher-concentration $MgCl_2$ brine appears to dissolve more material along exposed edges, resulting in shorter continuous edges. However, in the sulfate experiments a unique "chaotic honeycomb" texture becomes more prevalent with increasing $MgSO_4$ concentration, particularly in the 3M $MgSO_4$ brine. This texture is evenly distributed across recognizable grain surfaces in the 1M $MgSO_4$ experiment, while the texture obscures most of the original grain surfaces in the 3M $MgSO_4$ samples. To our knowledge, this texture has not been reported in similar carbonate dissolution experiments (e.g., Duckworth & Martin 2004; Offeddu et al. 2014), suggesting that this texture may be unique to siderite dissolution in $MgSO_4$. The EDX spectra collected from these "chaotic honeycomb" textures are consistent with an iron carbonate phase and are not notably enriched in Fe, Mn, Mg, or SO_4. This suggests that these textures could form due to siderite dissolution, reprecipitation of siderite, or precipitation of another iron carbonate phase such as chukanovite (Pekov et al. 2007; Jiang & Tosca 2019).

The EDX spectra of these neutral experiments show iron enrichments and depletions on some grain surfaces, relative to the unreacted siderite, in both brine compositions. Mn also was enriched and depleted, relative to the starting material, on the surface of the reacted grains correlating strongly with Fe in all of the neutral experiments (Figure 4). The enrichment or depletion of Fe/Mn does not correlate with any textural changes. Calcium is not enriched in any observed sample from the neutral experiments. Additionally, Mg was generally depleted in the remaining siderite rather than enriched after reaction in all of the chloride experiments and in the 0.01M $MgSO_4$ experiment; however, Mg was enriched on grain surfaces in both the 1M and 3M $MgSO_4$ experiments.

While abundant solid material remained in the reactors after 15 weeks of dissolution in the neutral pH brines, very little or no solid material remained after 7 weeks in the unadjusted pH($\leqslant$2) experiments. In order to compare siderite surface textures between the neutral pH and acidic experiments, we conducted a separate 1 day dissolution experiment using the same pH $\leqslant 2$ $MgCl_2$ and $MgSO_4$ concentrations used in the 7 week dissolution experiments. In these short-term acidic experiments, we did not observe the unique chaotic texture detected in the neutral $MgSO_4$ experiments. Instead we observed dissolution features that appear to cut through the siderite grains along crystallographically oriented planes in all six brines at pH $\leqslant 2$. These planar dissolutions features are not detected in the neutral experiments. The acidic experiments showed this grain-scale cross-cutting dissolution after only 1 day in solution.

Finally, we analyzed solid reaction products with Raman spectroscopy from both acidic and neutral experiments after

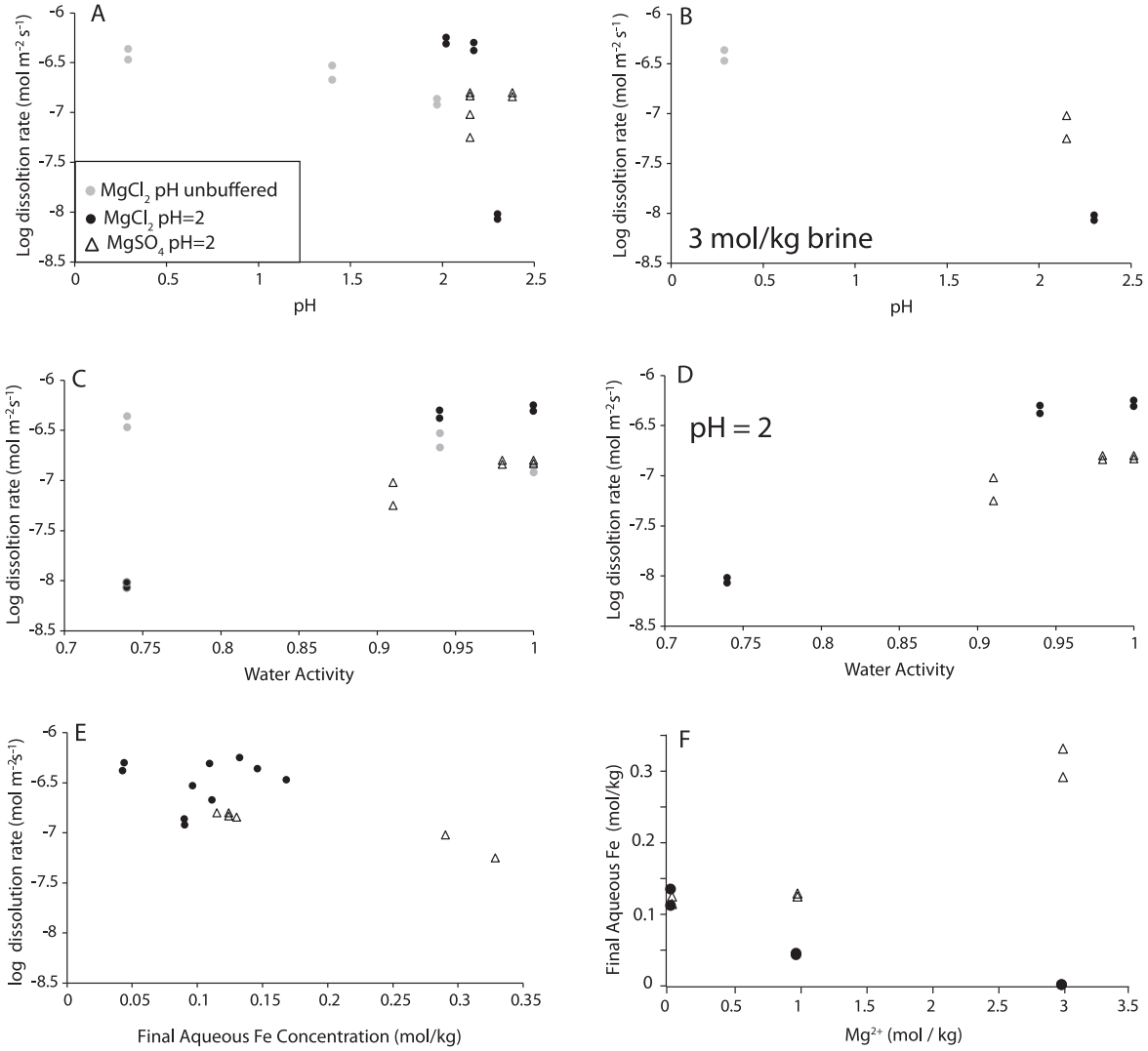

Figure 2. Initial siderite dissolution rates in acidic brines with different compositions ($MgCl_2$ circles, $MgSO_4$ diamonds) and concentrations. Black shapes represent increasing concentration of salt at pH ~2; gray circles represent initial $MgCl_2$ experiments that produced significantly more acidic conditions in the 3 mol kg^{-1} solutions. Initial iron release rates were relatively constant as a function of pH (A) except in the highest-concentration pH 2 brine experiments, suggesting initial siderite dissolution rates decrease in high $MgSO_4$ and $MgCl_2$ concentration brines. Dissolution rates were similar in the highest-concentration sulfate and chloride brines at pH = 2, but were faster at lower pH conditions in the unbuffered $MgCl_2$ brine experiments (B). In unadjusted $MgCl_2$ (pH = 0.29) the initial iron release rate observed in the 3M $MgCl_2$ solution was comparable to the more dilute solutions with pH 1.4–1.9 (C). Initial iron release rates decreased only slightly as the activity of water decreased from 1 to 0.9 in both brines under constant pH conditions but decreased significantly in the 3M $MgCl_2$ brine experiments at pH 2 (D). Final iron concentrations decrease with increasing dissolution rate at pH 2 (E), likely due to precipitation of secondary iron (hydr)oxides. Final iron concentrations increased with salt concentration and were higher in the sulfate brines compared to the chloride brines, where final iron concentrations decreased in the higher salinity brines (F)).

(The data used to create this figure are available.)

552 days and 364 days, respectively (Figure 5). These spectra indicate iron (hydr)oxide precipitation, as well as some remaining siderite in each of the different brine experiments.

4. Discussion

4.1. Dissolution Rates

Dissolution readily occurred in the acidic brines, allowing for initial rates to be determined. In both $MgCl_2$ and $MgSO_4$ brines, salt concentration affected the initial dissolution rates in similar ways. Siderite dissolution rates in $MgSO_4$ appear to remain constant as concentration increases between 0.01 M and 1 M, then decrease significantly between 1 M and 3 M (Table 1; Figure 2), likely due to the decrease in the activity coefficient of water from about 0.98 in the 1 M solution to 0.91 in the 3 M solution (Guendouzi et al. 2003). This is a much more significant decrease in the activity of water than between the 0.01 M and 1 M brines (1–0.98). Similarly, the final amount of Fe in solution at the end of the experiments was lowest in both the 0.01 M and 1 M $MgSO_4$ brines but 2–3 times higher in the 3 M brine (Table 1). Higher Fe concentrations in the high-salinity sulfate brine possibly results from the formation of complexes between iron and sulfate. This effectively reduces the aqueous Fe activity in solution, allowing for more Fe to be released from the surface of the siderite grains before the solution reaches saturation.

Similar to the sulfate experiments, in the chloride pH = 2 experiments siderite dissolution rates decreased with increasing $MgCl_2$ concentration, likely due to similar changes in water activities (0.94 in 1 M $MgCl_2$, 0.74 in 3 M $MgCl_2$; Ha &

Table 1
Initial Siderite Dissolution Rates and Final Aqueous Fe in pH 2 $MgCl_2$ and $MgSO_4$ Brines with Corresponding Water Activities

Solute	Concentration (mol kg^{-1})	α_w[a]	Initial pH	Final Fe Concentration (mmol kg^{-1})	Log Initial Dissolution Rate (mol s^{-1} m^2)
$MgCl_2$	0.01	1	2.02	109.4	−6.31
$MgCl_2$	0.01	1	2.02	132.3	−6.25
$MgCl_2$	1	0.94	2.17	42.7	−6.38
$MgCl_2$	1	0.94	2.17	43.7	−6.3
$MgCl_2$	3	0.74	2.3	0.05	−8.07
$MgCl_2$	3	0.74	2.3	0.98	−8.02
$MgCl_2$	0.01	1	1.97	90.3	−6.92
$MgCl_2$	0.01	1	1.97	89.8	−6.86
$MgCl_2$	1	0.94	1.4	111.1	−6.67
$MgCl_2$	1	0.94	1.4	96.3	−6.53
$MgCl_2$	3	0.74	0.29	168.3	−6.47
$MgCl_2$	3	0.74	0.29	146.0	−6.36
$MgSO_4$	0.01	1	2.15	123.9	−6.83
$MgSO_4$	0.01	1	2.15	114.7	−6.8
$MgSO_4$	1	0.98	2.38	123.9	−6.8
$MgSO_4$	1	0.98	2.38	129.9	−6.84
$MgSO_4$	3	0.91	2.15	328.5	−7.25
$MgSO_4$	3	0.91	2.15	290.3	−7.02
H_2O[b]	0	1	2.5	⋯	−5.7
H_2O[b]	0	1	2.3	⋯	−5.8
H_2O[b]	0	1	2.0	⋯	−5.5

Notes.
[a] $MgCl_2$ activity of water from Ha & Chan (1999), $MgSO_4$ activity of water from Guendouzi et al. (2003).
[b] Siderite dissolution rates at similar pH, temperature, and pCO_2 conditions reported by Golubev et al. (2009).

Chan 1999) compared to the sulfate brine. The final concentrations of Fe in the chloride brine experiments decrease with increasing salt concentration under similar initial pH conditions (Table 1; Figure 2). However, in the pH < 2 chloride experiments, the increasing acidity with brine strength results in an increase in final concentration. Iron release rates in 0.01 M and 1 M $MgCl_2$ were faster than any of the observed sulfate rates, likely due to Fe-Cl complexation (Sidhu et al. 1981; Pritchett et al. 2012), but in 3 M $MgCl_2$ initial dissolution occurred about an order of magnitude slower. Overall, water activities are more drastically decreased by $MgCl_2$ than by $MgSO_4$ (Ha & Chan 1999; Guendouzi et al. 2003). In both brines, dissolution rates are inhibited by the lower activity of water with increasing brine strength (as low as 0.74 in our chloride solutions and 0.91 in our sulfate solutions). As water activity decreases, final Fe concentrations in $MgCl_2$ also decrease, whereas in $MgSO_4$ they increase.

Previous calcite/dolomite dissolution experiments in acidic sulfate brines observed gypsum precipitation on the surface of the crystal faces that slowed the dissolution rate (Wilkins et al. 2001; Huminicki & Rimstidt 2009; Offeddu et al. 2014). Ca^{2+} is a trace cation substituting for Fe in our siderite sample; however, EDX spectra and SEM imaging of siderite surfaces do not indicate that $CaSO_4$ is forming as a reaction product. Instead, we observed discrete solitary or twinned crystals of $BaSO_4$ on the surface, which appear to have formed in solution rather than precipitating on the mineral surface. However, gypsum precipitation is more likely to occur in mixed composition carbonates with higher Ca content commonly observed on Mars (Hausrath & Olsen 2013), in Martian dust (Bandfield et al. 2003), and within Mars meteorites (Bridges et al. 2001) than in siderite with only trace Ca^{2+}, and may result in decreased dissolution rates.

Dissolution rates in both $MgCl_2$ and $MgSO_4$ brines measured in these experiments are one to two orders of magnitude slower than previously derived rates under similar pH and temperature conditions, but without brines (Golubev et al. 2009, Table 1). Both studies report siderite dissolution rates normalized to surface area using the BET method; however, rate comparison between studies is speculative even under identical conditions (Morse et al. 2007), so the difference in magnitude may or may not be a result of brine presence. Indeed, the activity of water in the 0.01 M solutions is not significantly different from ultrapure water, and therefore should not lead to a large difference in dissolution rates. Instead, the ∼0.5 order of magnitude difference in rates between the previously reported dilute experiments (Golubev et al. 2009) and our 0.01M experiments may be due to differences in mixing mechanisms, iron measurement techniques, or other attributes of the experimental design.

4.2. Reaction Products

Low aqueous Fe concentrations observed in the near-neutral experiments were likely due to Fe (hydr)oxide precipitation in both chloride and sulfate brines. The phase(s) precipitating are likely hematite, lepidocrocite, or ferrihydrite based on our Raman spectra collected after ∼15 weeks (Figure 5) compared with other spectra in the literature (Mazzetti & Thistlethwaite 2002; Hanesch 2009). The spectra in the literature contain broad peaks centered between ∼650 and ∼750 wavenumbers, though this varies based on crystallinity of the mineral and experimental conditions. Some of our spectra contain similar broad peaks along with others indicative of other iron oxides. Ferrihydrite in our experiments likely precipitated due to the diffusion of oxygen into samples, as oxic conditions favor the precipitation of ferric iron oxides (Duckworth & Martin 2004) and other carbonates rather than siderite when other cations are available (Hausrath & Olsen 2013). Previous studies have suggested that precipitating

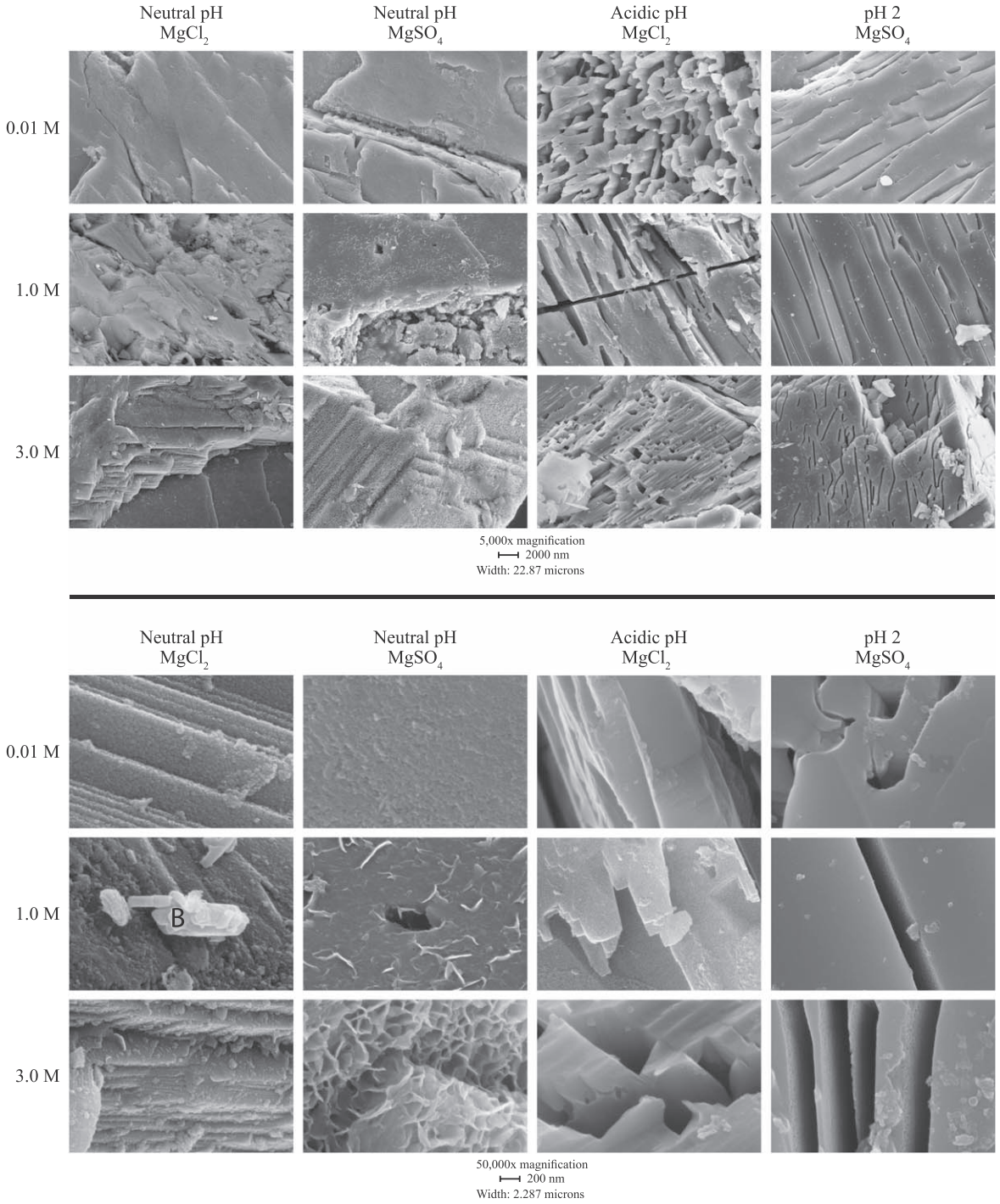

Figure 3. Representative secondary SEM images from each sample. Upper images were acquired at 5000 magnification and lower at 50,000 magnification; the scale bars below each magnification group apply to all the images within that group. In the near-neutral pH experiments the texture becomes rougher and less uniform as the $MgCl_2$ concentration increases. In the neutral sulfate experiments, increasing brine strength led to an extensive "chaotic honeycomb" texture. In the 1 day acidic (unadjusted pH) $MgCl_2$ experiments used to obtain images, all experiments produced channels and pits that appear oriented to the crystal structure. Lighter grains in the 1.0M neutral $MgCl_2$ images are representative of barite grains (B) found in the other experiments.

Fe-oxides can form a coating around grains, preventing further dissolution due to the relatively low solubility of iron oxides compared to the reacting phases (Duckworth & Martin 2004; Huminicki & Rimstidt 2008). Here we observe iron-rich granules (Figure 3) rather than an overall Fe enrichment of the surface, implying that in the case of the neutral experiments the lack of Fe in solution is not due to oxide coatings impeding siderite dissolution, but is instead due to precipitation of iron (hydr)oxides from solution following slight siderite dissolution. These (hydr)oxides are also typically enriched in Mn, which is found as a trace constituent in the unaltered siderite. This suggests that manganese, in addition to iron, concentrates as reprecipitation occurs. Conversely, the siderite surfaces are depleted in calcium and magnesium relative to the starting material, suggesting that in both chloride and sulfate brines Ca and Mg tend to remain in solution while Fe and Mn precipitate.

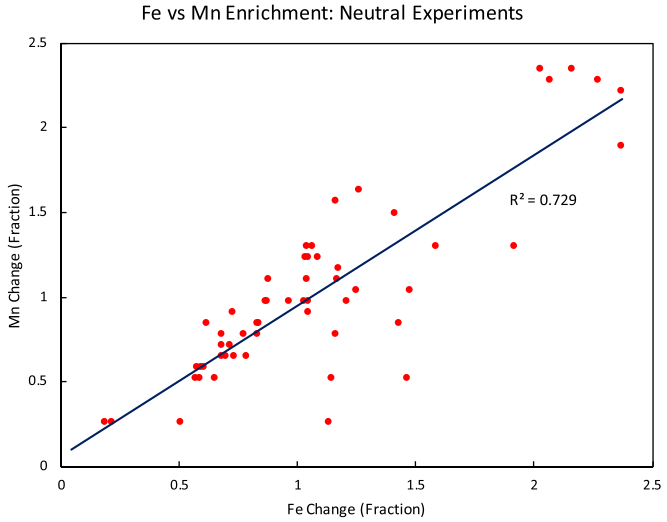

Figure 4. Mn enrichment plotted against Fe enrichment observed on the surface of the near-neutral-pH experiments. Values are represented as fractions relative to the composition of the raw siderite sample. A correlation exists with $R^2 = 0.729$ and a model F-statistic of 145.3, which implies that a linear model between Mn and Fe is informative from a statistical perspective. Residuals are distributed normally ($p = 0.004$) and have an rms error of 205.18%. No significant change was observed between trends in the sulfate vs. the chloride brines.

After 364 days, the broad Raman peak indicative of ferrihydrite around 700 wavenumbers disappears and instead we see peaks indicative of hematite (410 cm^{-1}) or goethite (385 cm^{-1}). Yee et al. (2006), Schwertmann & Murad (1983), and Liu et al. (2008) observed that ferrihydrite is unstable and alters to other more stable (hydr)oxides near room temperature. Liu et al. (2008) also observed that in the presence of Cl^-, lepidocrocite preferentially forms, whereas in the presence of SO_4^{2-}, goethite is observed; however, they also observe that at a pH below 7 goethite preferentially forms in both systems. However, we do not see strong evidence of a lepidocrocite/goethite dichotomy between our two brine anions. Kukkadapu et al. (2003) observed that six-line ferrihydrite readily forms under anaerobic neutral pH conditions, but that it may be an intermediate phase between the less organized two-line form and other Fe (hydr)oxides. Mazzetti & Thistlethwaite (2002) also observe that ferrihydrite variations in crystal structure and water content lead to variability in peak positions; the incorporation of other elements such as Mn would also influence Raman peak positions. Our results show that at about 15 weeks, ferrihydrite of some form (two-line or six-line) dominates the precipitated phases and after about 1 yr the ferrihydrite has altered to hematite, goethite, or other oxide phases. Additionally, our 364 day analyses of the neutral experiments indicate the lasting presence of siderite. However, some siderite is also still present even in the acidic experiments after 552 days. The remaining material in the acidic experiments is minuscule and grains large enough to obtain spectra are sparse; however, some still show a distinctive siderite peak (Figure 5) in addition to iron (hydr)oxide peaks. This may be due to the lower solubility of (hydr)oxides at moderate to slightly alkaline pH. We observe such an increase in our acidic experiments, and Duckworth & Martin (2004) show that precipitated iron oxide coatings on small grains may prevent dissolution. Instead of reaction sites being blocked, it may also be the case that in our closed-system reactors the pH and aqueous conditions changed such the system became saturated with respect to siderite. Additionally, an investigation into iron (III) oxide nucleation by Scheck et al. (2016) shows that at pH greater than 3 iron hydroxide precipitation depends on the size of prenucleation clusters, resulting in an increased precipitation rate once the complexes exceed a critical size. Therefore, as the pH increased in the acidic experiments over time, iron (hydr)oxide precipitation likely increased, perhaps shielding the remaining siderite from further dissolution.

Dependence on prenucleation processes has also been observed by Jiang & Tosca (2019) in their study of Fe(II)-carbonate precipitation. Here, they posit amorphous Fe-carbonates (AFCs) act as precursors for the precipitation of siderite and chukanovite. However, precipitation of carbonates only occurred at neutral-alkaline pH values (>7, with some dependence on pCO_2) and in highly saturated solutions. Thus, based on the near-neutral pH of our experiments we would not expect siderite or other Fe(II) carbonates to reprecipitate and we do not see any clear evidence of chukanovite or other ferrous carbonate phases on the surface of the samples in the Raman spectra (Figure 5). However, solubility experiments in high-salinity chloride brines indicate that chukanovite would be expected to form in systems less saturated in carbonate ions (Kim et al. 2017).

The textures of the neutral and acidic ($pH \leqslant 2$) experiments vary significantly (Figure 3). In the neutral experiments, we observe a unique texture in the $MgSO_4$ experiments, particularly at higher concentrations. This suggests anion chemistry is a critical factor in siderite dissolution texture, in addition to affecting dissolution rates at $pH \leqslant 2$. In the neutral chloride experiments, we observe more ragged edges and a rougher surface texture with higher concentrations of $MgCl_2$. In the short-term pH 2 experiments, variations in brine chemistry and concentration appear to have little effect on the surface texture. In all of the acidic experiments, planes cut through the surface of grains, likely along planes of weakness in the crystal structure, similar to cleavage surfaces. In the 3M chloride experiments, we see somewhat triangular and rhombohedral dissolution features on some surfaces that lack the linear dissolution channels (Figure 3). Textures such as the linear channeling and more angular pits seen in the 3M chloride brines have been well documented in carbonates (Morse et al. 2007). Offeddu et al. (2014) performed dissolution experiments on calcite and dolomite under pH 2–6 and low salinity conditions (5–50 mM Mg/Ca sulfate solutions), finding that rhombohedral pits formed in the (104) cleavage surface. Overall, the formation of the linear dissolution features likely increases surface area significantly, and therefore increases dissolution rate, especially as these features mature and cleave grains into multiple fragments.

We also observed barite in both the sulfate and chloride experiments (Figure 3). Assays provided by the chemical manufacturers indicate trace amounts of barium present substituting for Mg in both salts, so the precipitates observed here indicate that barite readily forms in brines even when Ba is only present in very trace amounts.

4.3. Implications for Mars

Given that Mars has a CO_2-rich atmosphere and an abundance of mafic rocks, one would expect carbon sequestration on the surface to be abundant. However, carbonates at the surface are less abundant than one would expect (Ehlmann & Edwards 2014). Neutral-alkaline conditions are thought to have

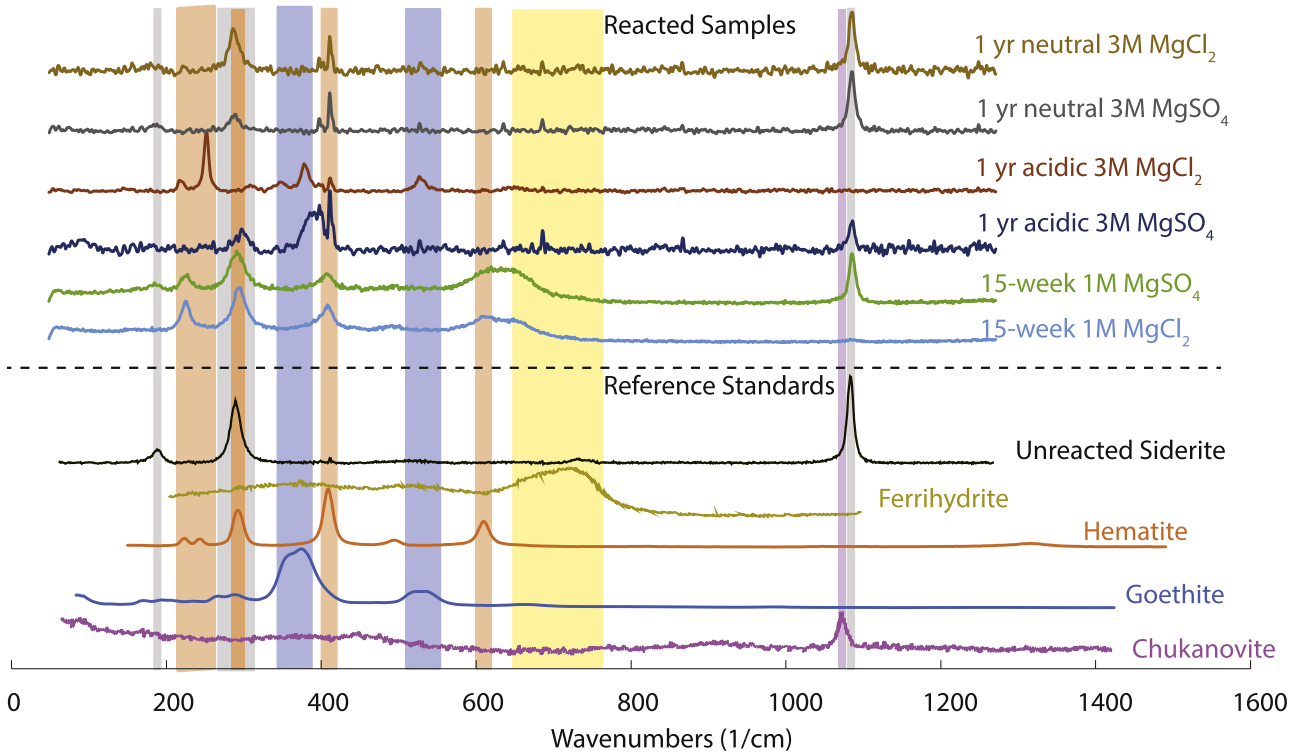

Figure 5. Raman spectra for unreacted siderite control, goethite (RRUFF database IDR050142), hematite (ID R040024), two-line ferrihydrite (Mazzetti & Thistlethwaite 2002), and chukanovite, as well as the reaction products produced in our experiments. The 15 week spectra are of the remaining material left to react in the neutral experiments for approximately 8 weeks after rate sampling was completed. Even after over 1 yr, the distinctive peak at around 1050 wavenumbers indicative of siderite remains in the acidic experiments. This is likely due to oxide coatings preventing total dissolution or due to an equilibrium being reached at higher pH conditions.

lasted until the late Noachian giving way to more acidic conditions during the Hesperian (Bibring et al. 2006; Ehlmann et al. 2008); however, carbonates in locations such as Nili Fossae (Ehlmann et al. 2009), the Phoenix landing site (Sutter et al. 2012), as well as Gusev Crater and Leighton Crater (Niles et al. 2013) suggest acidic conditions and soil pH are not homogeneous across Mars. Therefore, carbonates present on Mars today may have persisted through an overall acidic climate in localized areas of more neutral conditions.

Using the rates and textures derived in this study, we can provide context for interpreting the presence or absence of siderite in rocks and soils on Mars. In acidic $MgCl_2$ and $MgSO_4$ aqueous systems, we observed nearly complete dissolution of micron-sized siderite grains on a scale of 4–5 weeks in dilute brines. Under neutral conditions, we observed slow alteration that allows siderite to remain in solution for over a year. This suggests that rocks/soils that contain siderite and other carbonates likely have experienced little to no exposure to acidic brines, even for geologically short times. Planar-cutting features such as those observed in the acidic experiments may be an indicator for short-term acidic alteration, but also increase the surface area exposed to solution, thus speeding dissolution.

Previous studies have observed Fe-oxide and sulfate minerals coating carbonate grains, thus inhibiting further dissolution in previous studies (Wilkins et al. 2001; Duckworth & Martin 2004; Huminicki & Rimstidt 2009; Offeddu et al. 2014); we also saw evidence of coatings that would inhibit dissolution in these experiments. Particularly, in our long-term Raman analysis we observed peaks for hematite and goethite, as well as less common peaks for siderite in the same sample (Figure 5) which implies iron (hydr)oxide formation on the surface of grains. Under oxidizing conditions such as those in a CO_2 rich atmosphere (Fairén et al. 2004) capable of producing anhydrous oxidation (Ehlmann & Edwards 2014), this coating may prevent or slow dissolution of underlying carbonates in near-neutral pH solutions. On Mars, where carbonate assemblages are chemically heterogeneous (Hausrath & Olsen 2013), this may be more prevalent. For instance, a mixed Ca-/Fe-carbonate assemblage would be expected to lose the Ca component first because calcite generally has a higher dissolution rate than siderite (Hausrath & Olsen 2013). If alteration occurs in a sulfate-bearing fluid, gypsum may also precipitate, also preventing further dissolution of the underlying siderite.

From our experiments, we have determined dissolution rates for siderite under acidic brine conditions as well as reaction products and textures under neutral-pH brines of similar composition. This places experimentally derived limits on how siderite-bearing assemblages may be interpreted. Work by Wiesli et al. (2004) has shown that Fe isotope fractionation in siderite is controlled in part by dissolution rate; they found that slower precipitation and dissolution results in increased Fe fractionation. Therefore, iron isotope analyses of siderite samples in meteorites or on the surface of Mars could aid further interpretation of complex assemblages.

5. Conclusions

This study shows that acidic $MgCl_2$ and $MgSO_4$ brines can near-completely dissolve micron-scale siderite grains over days to weeks. Some siderite remains after over a year of acidic dissolution due to increasing pH with time and the formation of

iron (hydr)oxide grain coatings as a result of this increase. However, dissolution rates are much slower in neutral brines with considerable siderite remaining even after a year or more of dissolution.

Overall, increasing $MgCl_2$ concentrations resulted in slower siderite dissolution rates at pH 2 due to the lowering activity of water. Higher-concentration $MgCl_2$ in neutral brines also produced more ragged surface textures. However, dissolution rates in the pH 2 $MgSO_4$ brines slowed only in the highest-concentration brine (3M) likely due to a low activity of water (0.91). Neutral $MgSO_4$ brines produced increasing surface alteration as $MgSO_4$ concentration increased.

Siderite dissolved to form reaction products that include ferrihydrite, hematite, goethite, and other iron (hydr)oxides. Siderite in neutral conditions may last on geologic timescales but will likely show more complex compositions due to potential interaction with Ca^{2+}, Mg^{2+}, and Mn^{2+} from solution. In neutral conditions, we see Ca^{2+} depletion, suggesting that calcium phases do not reprecipitate as readily as other cation-bearing phases such as Fe-(hydr)oxides. The neutral experiments also show a texture unique to sulfate brines, suggesting that textural features may aid interpretations of aqueous chemistry.

The rapid dissolution of siderite in acidic brines further supports previous studies that suggested acidic alteration may have dissolved previously deposited Martian carbonates. Even under arid/cold conditions conducive to brines, a shift in Martian climate resulting in aqueous acid-sulfate weathering could plausibly dissolve siderite, even over geologically short periods of time, generating iron oxide reaction products.

Thank you to Dr. Savin for serving as editor and two anonymous reviewers whose comments improved this manuscript. Funding was provided by NASA grant #NNX13AG75G and the School of Geosciences at the University of Oklahoma. The authors would like to thank Dr. Preston Larson for his assistance in SEM/EDX analysis.

ORCID iDs

M. E. Elwood Madden https://orcid.org/0000-0002-6735-4554

References

Adcock, C. T., Hausrath, E. M., & Forster, P. M. 2013, NatGe, 6, 824
Altheide, T., Chevrier, V., Nicholson, C., & Denson, J. 2009, E&PSL, 282, 69
Bandfield, J. L., Glotch, T. D., & Christensen, P. R. 2003, Sci, 301, 1084
Bibring, J.-P., Langevin, Y., Mustard, J. F., et al. 2006, Sci, 312, 400
Bridges, J. C., Catling, D. C., Saxton, J. M., et al. 2001, SSRv, 96, 365
Clark, B. C., Morris, R. V., McLennan, S. M., et al. 2005, E&PSL, 240, 73
Cloutis, E. A., Craig, M. A., Mustard, J. F., et al. 2007, GeoRL, 34, L20202
Duckworth, O. W., & Martin, S. T. 2004, GeCoA, 68, 607
Ehlmann, B. L., & Edwards, C. S. 2014, AREPS, 42, 291
Ehlmann, B. L., Mustard, J. F., Murchie, S. L., et al. 2008, Sci, 322, 1828
Ehlmann, B. L., Swayze, G. A., Milliken, R. E., et al. 2016, AmMin, 101, 1527
Elwood Madden, M. E., Bodnar, R. J., & Rimstidt, J. D. 2004, Natur, 431, 821
Fairén, A. G., Fernández-Remolar, D., Dohm, J. M., Baker, V. R., & Amils, R. 2004, Natur, 43, 423
Gendrin, A., Mangold, N., Bibring, J. P., et al. 2005, Sci, 307, 1587
Golubev, S. P., Bénézeth, P., Schott, J., et al. 2009, ChGeo, 265, 13
Guendouzi, M. EL., Mounir, A., & Dinane, A. 2003, Chemical Thermodynamics, 35, 209
Ha, Z., & Chan, C. K. 1999, AerST, 31, 154
Hanesch, M. 2009, GeoJI, 177, 941
Hausrath, E. M., & Olsen, A. A. 2013, AmMin, 98, 897
Huminicki, D. M. C., & Rimstidt, J. D. 2009, ApGc, 24, 1626
Huminicki, D. M. C., & Rimstidt, J. D. 2008, ApGc, 23, 148
Jiang, C. Z., & Tosca, N. J. 2019, E&PSL, 506, 231
Kim, S., Marrs, C., Nemer, M., & Je-Hun Jang, J. 2017, ESC, 1, 647
Kukkadapu, R., Zachara, J., Fredrickson, J., et al. 2003, AmMin, 88, 1903
Lafuente, B., Downs, R. T., Yang, H., & Stone, N. 2015, Highlights in Mineralogical Crystallography (Berlin: W. De Gruyter), 1
Liu, H., Guo, H., Li, P., & Wei, Y. 2008, JSSCh, 181, 2666
Martín-Torres, F. J., Zorzano, M., Valentín-Serrano, P., et al. 2015, NatGe, 8, 357
Mazzetti, L., & Thistlethwaite, P. J. 2002, JRSp, 33, 104
Miller, J. L., Elwood Madden, A. S., Phillips-Lander, C. M., Pritchett, B. N., & Elwood Madden, M. E. 2016, GeCoA, 172, 93
Morris, R. V., Ruff, S. W., Gellert, R., et al. 2010, Sci, 329, 421
Morse, J. W., Arvidson, R. S., & Lüttge, A. 2007, ChRv, 107, 243
Niles, P. B., Catling, D. C., Berger, G., et al. 2013, SSRv, 174, 301
Offeddu, F. G., Cama, J., Soler, J. M., & Putnis, C. V. 2014, Beilstein Journal of Nanotechnology, 5, 1245
Ojha, L., Wilhelm, M. B., Murchie, S. L., et al. 2015, NatGe, 8, 829
Osterloo, M. M., Anderson, F. S., Hamilton, V. E., & Hynek, B. M. 2010, JGR, 115, E10012
Pekov, I. V., Perchiazzi, N., Merlino, S., et al. 2007, EJMin, 19, 891
Pritchett, B. N., Elwood Madden, M. E., & Madden, A. S. 2012, E&PSL, 357, 327
Rimstidt, J. D. 2014, Geochemical Rate Models: An Introduction to Geochemical Kinetics (Cambridge: Cambridge Univ. Press),
Rivera-Valentín, E. G., Chevrier, V. F., Soto, A., et al. 2020, NatAs, 4, 756
Scheck, J., Wu, B., Dreschler, M., et al. 2016, Physical Chemistry Letters, 7, 3123
Schwertmann, U., & Murad, E. 1983, CCM, 31, 277
Sidhu, P. S., Gilkes, R. J., Cornell, R. M., Posner, A. M., & Quirk, J. P. 1981, CCM, 29, 269
Squyres, S. W., Grotzinger, J. P., Arvidson, R. E., et al. 2004, Sci, 306, 1709
Sutter, B., Boynton, W. V., Ming, D. W., et al. 2012, Icar, 218, 290
Toner, J. D., Catling, D. C., & Light, B. 2014, Icar, 233, 36
Wang, A., Jolliff, B. L., Liu, Y., & Connor, K. 2016, JGRE, 121, 678
Wiesli, R. A., Beard, B. L., & Johnson, C. M. 2004, ChGeo, 211, 343
Wilkins, S. J., Compton, R. G., Taylor, M. A., & Viles, H. A. 2001, JCIS, 236, 354
Yee, N., Shaw, S., Benning, L. G., & Nguyen, T. H. 2006, AmMin, 91, 92
Yen, A. S., Gellert, R., Schröder, C., et al. 2005, Natur, 436, 49